

Limits to causal inference with state-space reconstruction for infectious disease

Sarah Cobey^{*1} and Edward B. Baskerville^{†1}

¹Ecology & Evolution, University of Chicago, Chicago, IL, USA

^{*}cobey@uchicago.edu

[†]edbaskerville@uchicago.edu

Abstract

Infectious diseases are notorious for their complex dynamics, which make it difficult to fit models to test hypotheses. Methods based on state-space reconstruction have been proposed to infer causal interactions in noisy, nonlinear dynamical systems. These “model-free” methods are collectively known as convergent cross-mapping (CCM). Although CCM has theoretical support, natural systems routinely violate its assumptions. To identify the practical limits of causal inference under CCM, we simulated the dynamics of two pathogen strains with varying interaction strengths. Traditional CCM is extremely sensitive to periodic fluctuations, inferring interactions between independent strains that oscillate with similar frequencies. This sensitivity vanishes with alternative criteria for inferring causality. However, CCM in general is sensitive to high levels of process noise and deviations from steady-state dynamics. This sensitivity is problematic because it remains challenging to measure (and even define) noise and nonequilibrium behavior in natural systems, including the quality of reconstructed attractors that underlie cross-mapping. We illustrate these challenges by analyzing time series of reportable childhood infections in New York City and Chicago during the pre-vaccine era. We comment on the statistical and conceptual challenges that limit the use of state-space reconstruction in causal inference.

Keywords: demographic stochasticity, environmental stochasticity, attractor reconstruction, mechanistic models

1 Background

Identifying the forces driving change in natural systems is a major goal in ecology. Because experiments are often impractical and come at the cost of generalizability, a common approach is to fit mechanistic models to observations. Testing hypotheses through mechanistic models has a particularly strong tradition in infectious disease ecology [1–4]. Models that incorporate both rainfall and host immunity, for example, better explain patterns of malaria than models with only rainfall [5]; models with school terms fit the historic periodicity of measles in England and Wales [6, 7]. The ability of fitted mechanistic models to predict observations outside the training data strongly suggests that biological insight can be gained. There is nonetheless a pervasive risk that predictive variables merely correlate with the true, hidden variables, or that the model’s functional relationships create spurious resemblances to the true dynamics. This structural uncertainty in the models themselves limits inference [8–11].

An alternative approach to inferring causality is to examine the time series of potentially interacting variables without invoking a model. These methods face a similar challenge: they must distinguish correlated independent variables sharing a mutual driver from correlations arising from direct or indirect interactions. Many of these methods infer interactions in terms of information flow and apply to simple, linear systems (e.g., [12]) or limited types of interactions (e.g., [13–15]). A recent suite of methods based on time series analysis proposes to infer interactions in systems that are noisy, nonlinear, and potentially high-dimensional [16–18]. The basic idea is that if X drives Y , information about X is embedded in the time series of Y . Examining the relationships between delay-embeddings of the time series of X and Y can reveal if the interaction is symmetric, asymmetric, or absent. These approaches, which we refer to collectively as convergent cross-mapping (CCM), have been offered as general tools to analyze causation in nonlinear systems [16–18].

The mathematical foundations of CCM, and therefore its assumptions, lie in deterministic nonlinear systems theory. After sufficient time, the states of a dynamical system reach an attractor, which may be a point equilibrium, a limit cycle, or a higher-dimensional chaotic attractor. By Takens’ theorem, a one-dimensional time series $X(t)$ from the system can be mapped perfectly to the attractor in the full state space in the system by constructing a delay embedding, in which states of the full system are mapped to delay vectors, $\mathbf{x}(t) = \{X(t), X(t - \tau_1), X(t - \tau_2), \dots, X(t - \tau_{E-1})\}$, for *delays* τ_i and an *embedding dimension* E , which must be at least as large as the dimensionality of the attractor [19]. This mapping provides the basis for causal inference under CCM: if Y drives (causes) X , then a newly observed $\mathbf{x}(t)$ can perfectly reconstruct the corresponding $\hat{Y}(t)$ from past observations of the mapping $\mathbf{x}(t) \rightarrow Y(t)$ (Fig. 1A). Convergence in CCM comes from the fact that, as the number of observed delay vectors $\mathbf{x}(t)$ increases, the reconstruction converges to arbitrarily small error, as observed points on the reconstructed attractor become arbitrarily close together [16].

With finite, noisy real data, the convergence is necessarily imperfect, and two operational criteria have been used to detect causality. The first criterion (Fig. 1B) is based simply on this improvement in reconstruction quality with the number of observations. This approach is known to produce false positives in the mathematically pathological case [16] of strongly driven variables, where the system becomes synchronized to the driver [20]. Note that this failure is logically consistent with the theory: the theory implies that, with perfect data, causal drivers will produce good reconstructions, but not that non-causal drivers will not produce good reconstructions. The second criterion (Fig. 1C) tries to correct this problem by additionally considering the directionality of information flow in time [17].

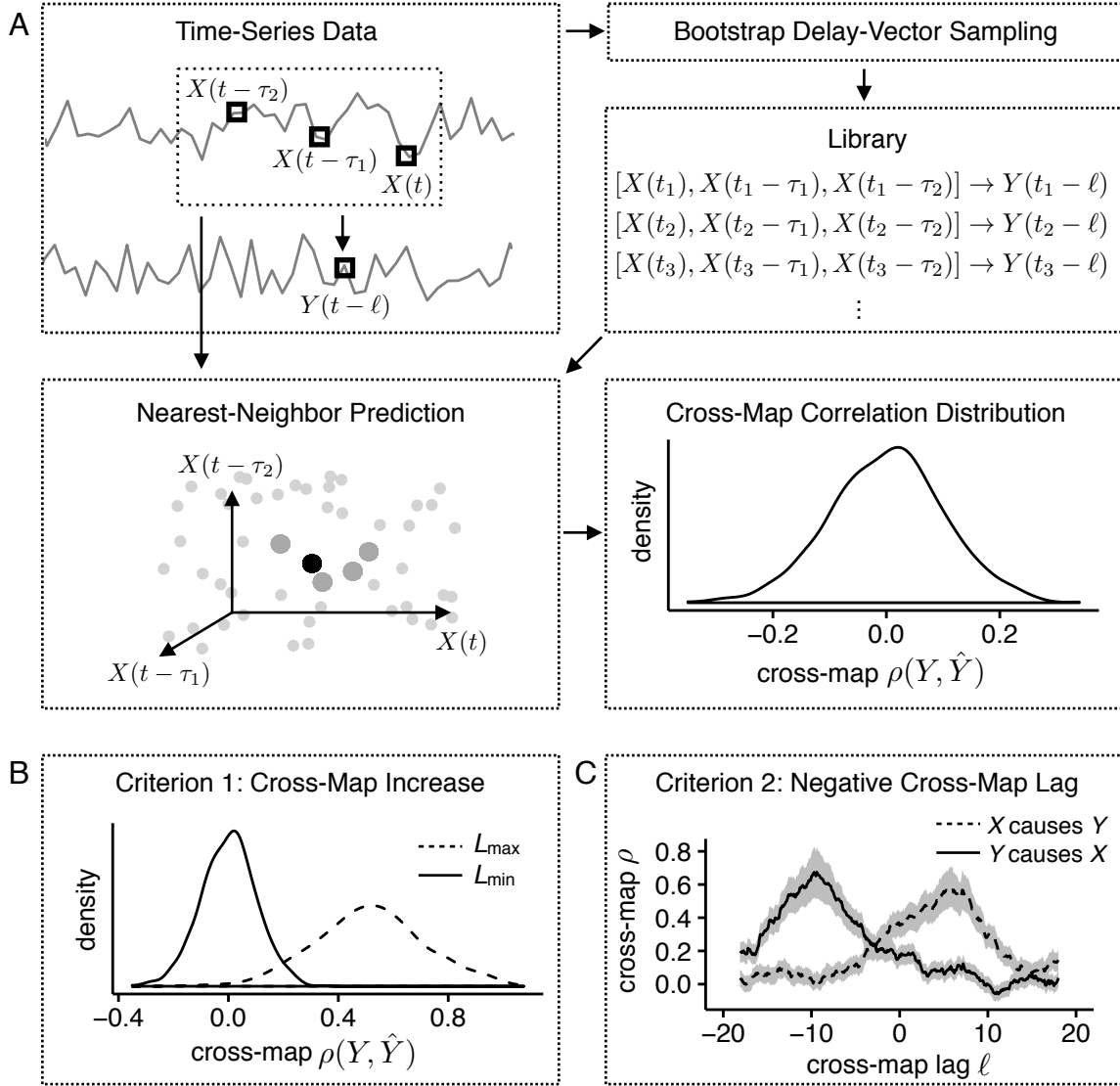


Figure 1: **Summary of criteria for detecting causality.** (A) Schematic of cross-map algorithm for testing $Y \rightarrow X$. Delay vectors in X , mapped to values in Y with lag ℓ , are bootstrap-sampled to construct a prediction library. For each delay vector in X , reconstructed values \hat{Y} are calculated from a distance-weighted sum of Y values from nearest neighbors in the library. Many sampled libraries yield a distribution of cross-map correlations between actual Y and reconstructed \hat{Y} . (B) Criterion 1 (cross-map increase). Bootstrap distributions of cross-map correlation are calculated at minimum and maximum library sizes with $\ell = 0$; causality is inferred if the correlation at L_{\max} is significantly greater than the correlation at L_{\min} . (C) Criterion 2 (negative cross-map lag). Cross-map correlations are calculated across different values of ℓ . Causality is inferred if the highest cross-map correlation for negative ℓ is positive and significantly greater than the highest value for nonnegative ℓ .

Many ecological systems undergo synchronized diurnal or annual fluctuations, in potentially pathological ways, and thus raise doubts about the first criterion. Nonstationarity, demographic and environmental noise, and observation error—all ubiquitous in nature—raise general concerns, since they violate the theory’s assumption that variables are perfectly observed at deterministic equilibrium. Variations of CCM have nonetheless been applied to such systems to test hypotheses about who interacts with whom [16–18, 21, 22].

We investigated whether the frequently periodic, noisy, and nonstationary features of ecological systems are a fundamental obstacle to causal inference based on state-space reconstruction. These factors have been addressed to varying degrees in different contexts [16–18] but not systematically. Specifically, we examined whether the two criteria for causal inference are robust to inevitable uncertainties about the dynamics underlying the data. With little prior knowledge of a system’s complexity, including the influences of nonstationarity and noise, can we reach statistically rigorous conclusions about who interacts with whom? Infectious diseases provide a useful test case because their dynamics have been extensively studied, long time series are available, and they display diverse immune-mediated interactions [23]. Their dynamics are also influenced by seasonal variation in transmission rates, host population structure, and pathogen evolution. The ability to test directly for the presence of interactions would save considerable effort over fitting elaborate semi-mechanistic models that incorporate these complexities. We find that although CCM appears to work beautifully in some instances, it does not in others. Noise and nonstationarity contribute to poor outcomes, as do fundamental ambiguities in the methodology itself.

2 Results

To assess the reliability of CCM, we began by simulating the dynamics of two strains with stochastic, seasonally varying transmission rates (Methods). The amount of process noise in natural time series is effectively never known (and is partly defined by the bounds placed on the system), and we consequently varied it. We also varied the strength of competition from strain 2 on strain 1 (σ_{12}); strain 1, in contrast, never affected strain 2 ($\sigma_{21} = 0$). For each level of competition and process noise, we simulated 100 replicates from random initial conditions to steady state. One thousand years of error-free monthly incidence were output to give CCM the best chance to work. For each combination of parameters (competition strength σ_{12} and process noise η), we examined whether strain interactions were correctly inferred. When $\sigma_{12} > 0$, strain 2 should be inferred to “drive” (influence) strain 1. Because $\sigma_{21} = 0$, strain 1 should never be inferred to drive strain 2.

To detect interactions, for each individual time series, we identified the delay-embedding (Fig. 1A) and applied one of two causality criteria using the reconstructed attractors (Fig. 1B,C and Methods). Both criteria are based on the cross-map correlation ρ , which is the correlation between reconstructed values of \hat{Y} and actual values of Y , given the reconstructed attractor of X . Criterion 1 [16, 18] measures whether the cross-map correlation increases as the number of observations of the putatively driven variable grows (Fig. 1B). We refer to this as the cross-map increase criterion. Criterion 2 [17] infers a causal interaction if the maximum cross-correlation of the putative driver is positive and occurs at a negative temporal lag (Fig. 1C). We refer to this as the negative cross-map lag criterion. For simplicity, we start with Criterion 1.

2.0.1 Sensitivity to periodicity

Criterion 1, which requires a significant increase in cross-map correlation ρ with observation library size L , frequently detected interactions that did not exist. Strain 2 was always incorrectly inferred to drive strain 1 in simulations when it did not (Fig. 2A). Although strain 1 never influenced strain 2, it was often predicted to (Fig. 2A). Sample time series suggested a strong correlation between synchronous oscillations and the appearance of bidirectional interactions (Fig. 2B). In contrast, when strain 2 appeared to drive strain 1 but not vice-versa ($\sigma_{12} = 0$ and $\eta = 0.05$), strain 1 often oscillated in phase with strain 2 but at a lower frequency (Fig. 2C). Thus, as expected, strongly synchronized dynamics prevented separation of the variables. Additionally, the resemblance of strain 2 to the seasonal driver led to false positives even when the strains were independent and strain 1 oscillated at a different frequency.

The sensitivity of the method to periodicity persisted despite transformations of the data and changes to the driver. One possible solution to reducing seasonal effects, sampling annual rather than monthly incidence, reduced the overall rate of false positives but also failed to detect some interactions (Fig. S1A). Furthermore, when the effects of strain 2 on 1 were strongest, the reverse interaction was more often inferred. Sampling the prevalence at annual intervals gave similar results (Fig. S1B), and first-differencing the data did not qualitatively change outcomes (Fig. S1C). The method yielded incorrect results even without seasonal forcing ($\epsilon = 0$) because of noise-induced oscillations (Fig. S1D). In all of these cases, the presence of shared periods between the strains correlated strongly and significantly with the rate of detecting a false interaction (Fig. 3).

Because cross-map skill should depend on the quality of the reconstructed attractor, we investigated performance under other methods of constructing \mathbf{M}_{C_1} and \mathbf{M}_{C_2} (Methods). Nonuniform embedding methods allow the time delays to occur at irregular intervals, $\tau_1, \tau_2, \dots, \tau_{E-1}$, which may provide a more accurate reconstruction. Alternative reconstruction methods, including nonuniform embedding [24,25], random projection [21], and maximizing the cross-map (rather than univariate) correlation failed to fix the problem (Fig. S2).

Criterion 2, which infers that Y drives X if there is a positive cross-map correlation that is maximized at a negative cross-map lag, performed relatively well (Fig. 4). Fewer false positives were detected, although the method missed some weak extant interactions ($\sigma_{12} = 0.25$) and interactions in noisy systems ($\eta = 0.05, 0.1$). Results for annual data were similar (Fig. S3A). Requiring that ρ be not only positive but also increasing barely affected performance (Fig. S3B).

2.0.2 Limits to identifiability

If two variables X and Y share the same driver but do not interact, at some limit, X may resemble the driver so strongly that X appears to drive Y . In a similar vein, when the two strains in our system have identical transmission rates ($\beta_1 = \beta_2$) and one strongly drives the other ($\sigma_{12} = 1$), the direction of the interaction cannot be detected when the dynamics are nearly deterministic ($\eta = 10^{-6}$) (Fig. S3C). Causal inference in such cases becomes difficult.

To investigate the limits to distinguishing ecologically similar, non-interacting strains, we varied the correlation of the strain-specific process noise while applying the more conservative of the two criteria for inferring causality (Criterion 2), that the cross-map correlation ρ be positive and peak at a negative lag [17]. Process noise can be thought of as a hidden environmental driver that affects both strains simultaneously,

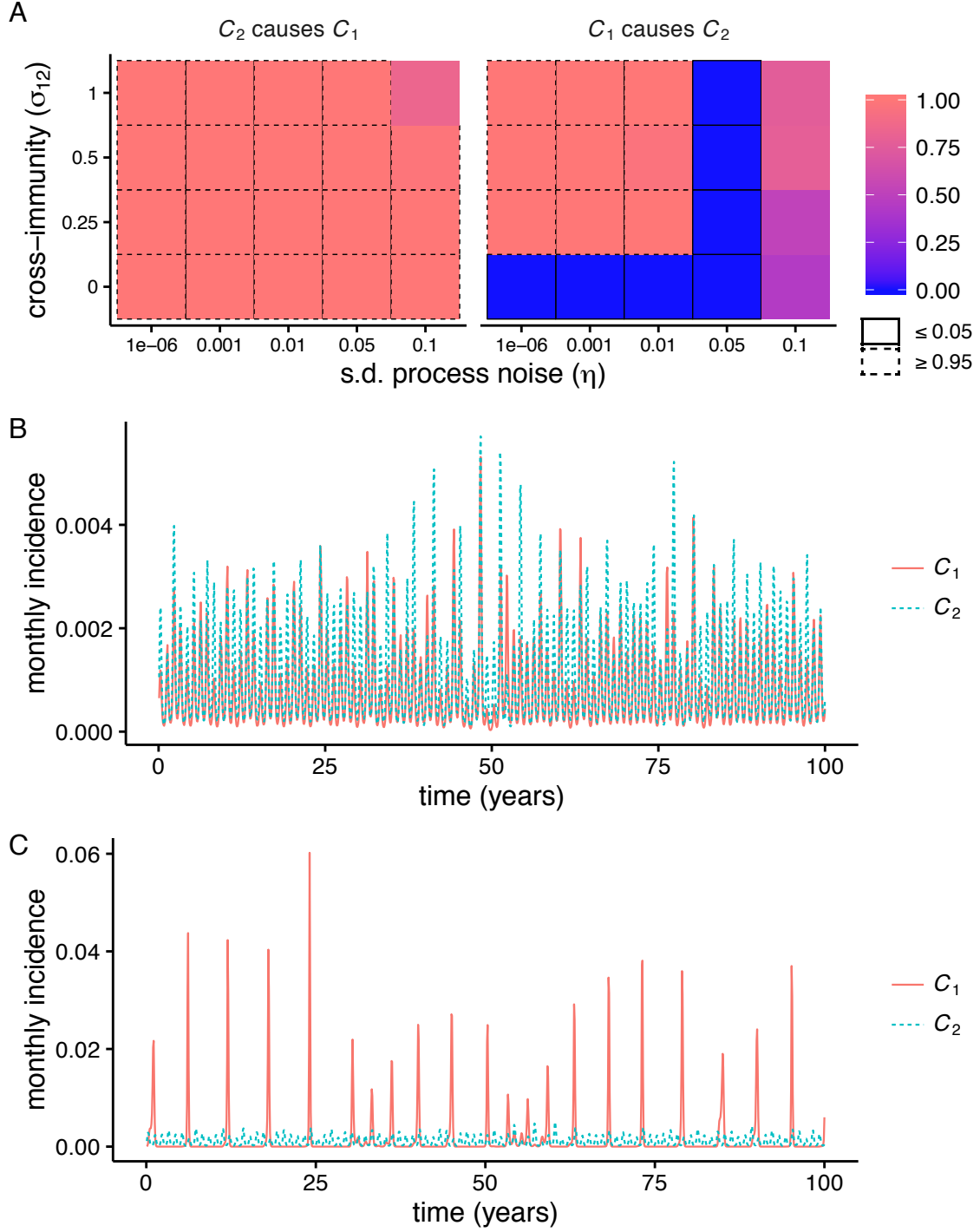


Figure 2: **Interactions detected as a function of process noise and the strength of interaction ($C_2 \rightarrow C_1$) and representative time series.** (A) Heat maps show the fraction of 100 replicates significant for each inferred interaction for different parameter combinations. A significant increase in cross-map correlation ρ with library length L indicated a causal interaction. (B) Representative time series for which mutual interactions were inferred ($\sigma_{12} = 0.25, \eta = 0.01$). (C) Representative time series for which C_2 is inferred to drive C_1 but not vice-versa ($\sigma_{12} = 0.25, \eta = 0.05$).

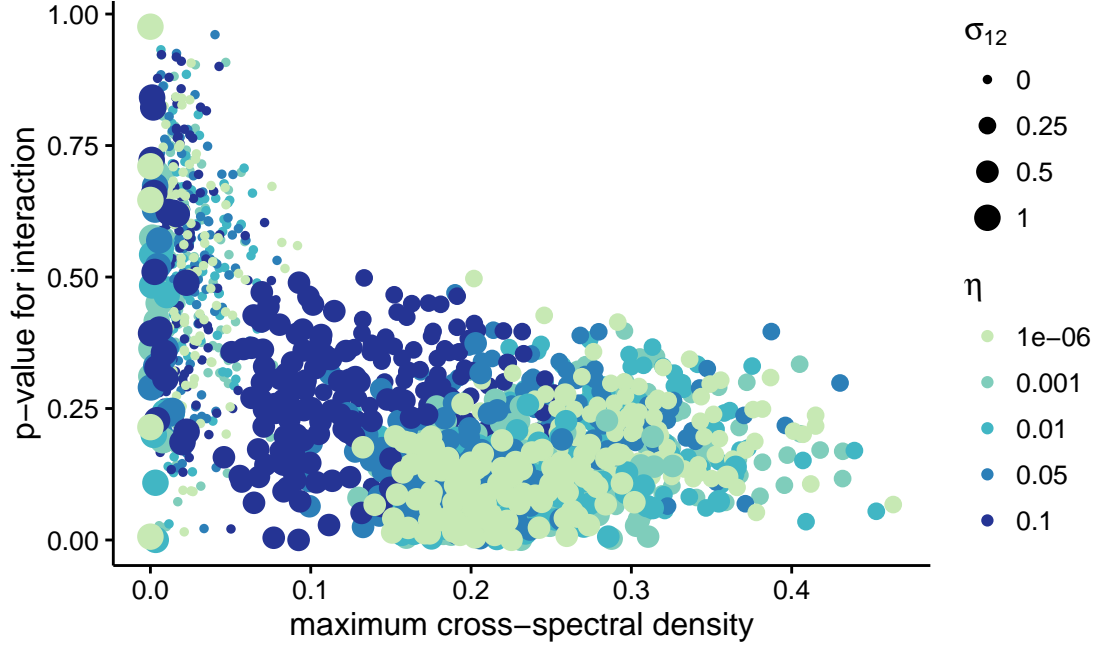


Figure 3: **Shared frequency spectra predict probability of inferred interaction.** Points show the maximum cross-spectral densities of strains 1 and 2 plotted against the p-values for $C_1 \rightarrow C_2$. In all replicates, C_1 never actually drives C_2 . Point color indicates the strength of $C_2 \rightarrow C_1$ (σ_{12}), and point size indicates the standard deviation of the process noise (η) on transmission rates.

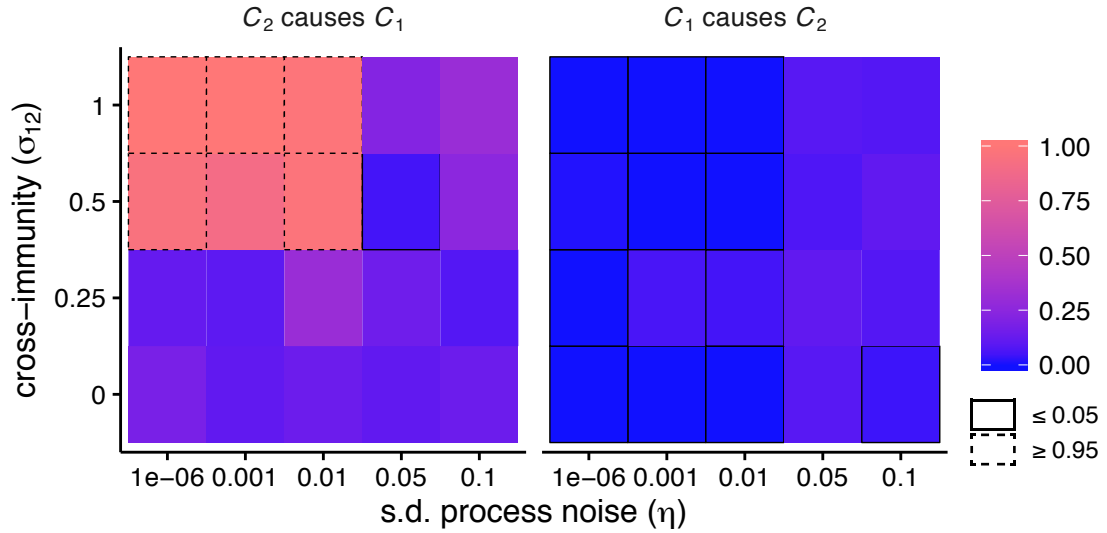


Figure 4: **Interactions detected as a function of process noise and the strength of interaction ($C_2 \rightarrow C_1$) and representative time series.** Heat maps show the fraction of 100 replicates significant for each inferred interaction for different parameter combinations. A maximum, positive cross-map correlation ρ at a negative cross-lag indicated a causal interaction. Each replicate used 100 years of monthly incidence.

and thus the strength of correlation indicates the relative contribution of shared versus strain-specific noise. With two identical, independent strains and low process noise ($\eta = 0.01$), the false positive rate varied non-monotonically with the correlation strength. It peaked at approximately 19%-24% with perfectly correlated noise and reached a minimum at a correlation of 0.75 (Fig. S4A). Analyzing annual instead of monthly incidence, or applying Criterion 2 rather than Criterion 1, reduced the false positive rate to $< 5\%$ for imperfectly correlated noise (Fig. S4B, C). Thus, the independence of two strains will generally be detected as long as they experience imperfectly correlated noise.

We next considered the problem of identifying two ecologically distinct strains ($\beta_1 \neq \beta_2$) when one strain strongly drives the other ($\sigma_{12} = 1$) and its dynamics resemble the seasonal driver. In this case, even with perfectly correlated process noise, correct interactions are consistently inferred (Fig. S5). Thus, we conclude that the presence of noise, even highly correlated noise, can help distinguish causality between coupled, synchronized variables. It is more difficult to distinguish non-interacting, dynamically equivalent variables. In the latter case, noise has inconsistent effects on causal inference, although Criterion 2 may perform much better than Criterion 1. These results at least hold for “modest” noise ($\eta = 0.01$): as shown earlier, higher levels hurt performance (Fig. 4).

2.0.3 Non-steady-state dynamics

CCM assumes steady-state dynamics, and deviations from steady-state should compromise the integrity of the reconstructed attractors. Our results have shown that the method, under Criterion 2, is robust to, and even benefits from, relatively low noise, but severe deviations from equilibrium behavior could limit effective cross-mapping. As a proof of principle, we evaluated the impact of transient dynamics on causal inference. When strain 2 weakly drives strain 1 ($\sigma_{12} = 0.5$), causal inference is strongly affected (Fig. 5). In 100 simulations of this scenario, the correct interaction was always detected at steady state, but with transient dynamics it was detected in only 19 of 100 simulations. Furthermore, the incorrect interaction (strain 1 driving 2) was detected in 21 of 100 simulations. After log-transformation of the data, the correct interaction was detected in only 5 of 100 simulations, while the incorrect interaction was detected in 23 of 100 simulations.

2.0.4 Application to childhood infections

Given the success of CCM under Criterion 2 (negative cross-map lag) with two strains and little noise at steady state, we investigated whether the method might shed light on the historic dynamics of childhood infections in the pre-vaccine era. Time series analyses have suggested that historically common childhood pathogens may have competed or facilitated one another [26, 27]. We obtained the weekly incidence of six reportable infections in New York City from intermittent periods spanning 1906 to 1953 [28] (Fig. 6A). Six of 30 pairwise interactions were significant at the $p < 0.05$ level, not correcting for multiple tests (Fig. 6C). Polio drove mumps and varicella, scarlet fever drove mumps and polio, and varicella and pertussis drove measles. Typical cross-map lags occurred at one to three years (Fig. S6). The inferred interactions were identical if we required that the cross-map correlation ρ be increasing and not merely positive.

Although we specifically chose infectious diseases not subject to major public health interventions in the sampling period, it is possible that the New York data reflect non-steady-state dynamics. To check robustness of the conclusions, we analyzed analogous time series from Chicago from the same period (Fig. 6B).

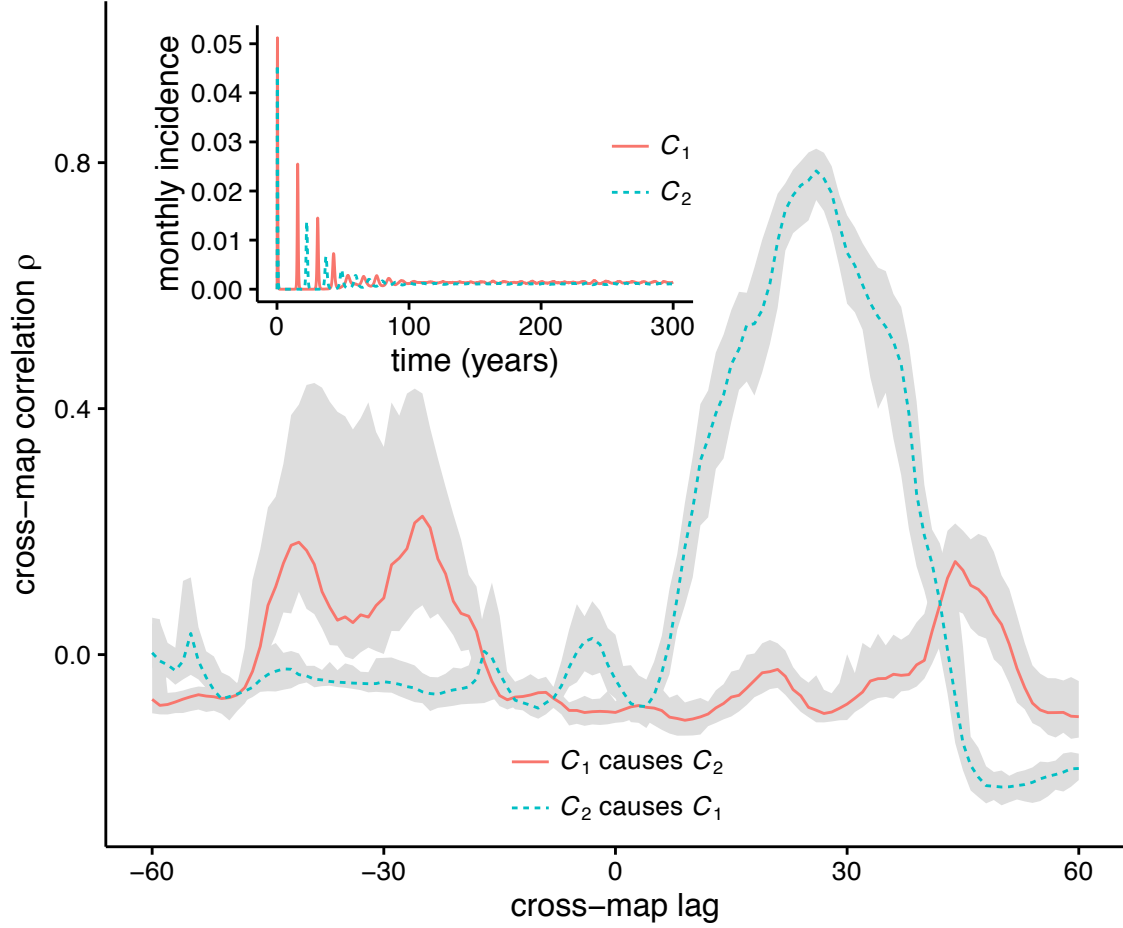


Figure 5: **Incorrect inference with transient dynamics.** Cross-map correlations at different lags for a sample time series (inset). Lines represent bootstrap medians; gray ribbons represent the middle 95% of the bootstrap distribution. Although C_2 drives C_1 ($\sigma_{12} = 0.5, \sigma_{21} = 0$), the maximum cross-correlation ρ for C_1 cross-mapped to C_2 occurs at a positive lag, and the reverse at a negative lag, leading to the conclusion that C_1 drives C_2 , and C_2 does not drive C_1 . Sample dynamics include process noise ($\eta = 0.01$) but no seasonal forcing ($\epsilon = 0$).

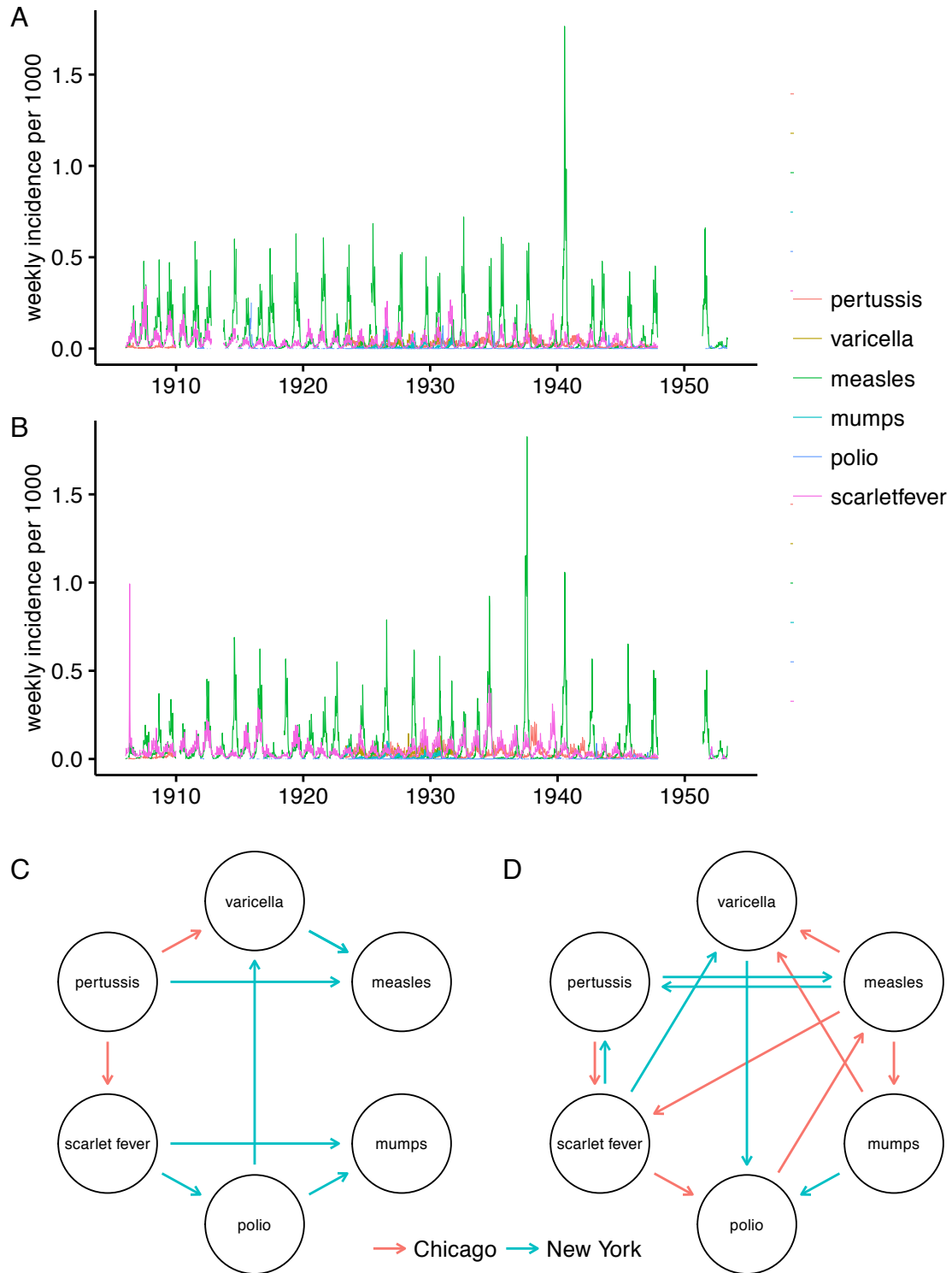


Figure 6: **Historical childhood infections in New York City and Chicago and inferred interactions from two reconstruction methods.** Time series show weekly incidence of infections per 1000 inhabitants of New York City (A) and Chicago (B). Delay-embeddings were constructed by maximizing the univariate correlation (C) or through a random projection method (D). Arrows indicate the inferred interactions from the New York (blue) and Chicago (red) time series under Criterion 2 (negative cross-map lag).

Completely different interactions appeared (Fig. 6C). Not correcting for multiple tests, pertussis drove scarlet fever and varicella; accepting marginally significant negative lags ($p = 0.055$), polio drove measles. In these cases, the maximum cross-map correlation ρ was not only positive but also increased at negative lag. Requiring that ρ only be positive at negative lag, polio also drove pertussis, measles drove mumps and varicella, and mumps drove scarlet fever. Except in one case, all negative lags occurred at more than one year (Fig. S7). Thus, no consistent interactions appeared in epidemiological time series of two major, and possibly dynamically coupled, cities.

To investigate the possibility that our method of attractor reconstruction might be unduly sensitive to noise and nonstationarity, we repeated the procedure with a method based on random projections [21]. Once again, no interactions were common to both cities (Fig. 6D). Furthermore, only one of the original eight interactions from the first reconstruction method reappeared with random projection (two of eight reappeared if disregarding the city), and two interactions changed direction (three if disregarding the city). Both reconstruction methods selected similar lags (Figs. S8, S9).

3 Discussion

CCM is, in theory, an efficient alternative to mechanistic modeling for causal inference in nonlinear systems. By evaluating properties of reconstructed attractors in state space, it sidesteps any need to formulate and fit what are often inaccurate mathematical models. In current practice, CCM appears an unstable basis for inference in natural systems. We simulated two interacting strains and found that the traditional CCM (Criterion 1) can lead to erroneous conclusions whenever strains fluctuated at similar frequencies. Applying a more recently proposed criterion for causality that considers the temporal lag at which the cross-map correlation is maximized [17], rather than the change in the cross-map correlation with time series length L [16], avoids this problem. Inference with Criterion 2 is somewhat robust to process noise, which can improve performance in some cases. But the method has two problems, even with perfect and abundant observations. First, it remains susceptible to deviations from its core dynamical assumptions. “High” process noise and non-steady-state dynamics each diminish performance, leading to false positives and negatives. Although some observed systems may be at deterministic equilibrium, this assumption is often dubious in ecology. Second, even when the dynamical assumptions are upheld, seemingly equally justifiable methods of attractor reconstruction yield different results. If the aim is to test hypotheses statistically, these problems raise questions about the suitability of any method based on state-space reconstruction in ecology.

Oscillations are common in nature, especially in infectious diseases, and suggest that the original criterion (Criterion 1) for causal inference could routinely mislead. Climatic and seasonal cycles, driven by such factors as school terms, El Niño, and absolute humidity, pervade the dynamics of many pathogens and influence the timing of epidemics [5, 6, 29–31]. Infectious diseases can also exhibit fluctuations in the absence of external forcing. These fluctuations arise from the well-known transient damped oscillations to equilibrium or from noise, which induces fluctuations on characteristic time scales and can interact with seasonal drivers to generate complex patterns [32–35]. Consumer-resource interactions [36–38] and patchy populations [39, 40] demonstrate similar behavior. In systems with possibly synchronized dynamics, the more reliable criterion for causal inference is a negative cross-map lag [17].

Assuming the stronger criterion for causality [17], under what conditions might we consider this method “safe”? At first glance, two situations cause concern. We have demonstrated that non-steady-state conditions

pose one difficulty. Although nonstationary or transient dynamics can sometimes be identified [41], and some forms of nonstationarity perhaps removed from the time series through first-differencing or detrending, not all forms of nonstationarity are identifiable or distinguishable from steady-state dynamics occurring over long time scales (e.g., a partially observed complex attractor). The other situation occurs when process noise is “high.” In our system, a $\geq 5\%$ standard deviation in the transmission rate generated appreciable false positives. Whether this rate is high or low relative to other systems is perhaps irrelevant, because there is no good way to define the impact of noise in a time series. One potential measure is the variance of the dynamics not explained by the deterministic skeleton, but without good information about the system (i.e., an accurate mechanistic model), the shape of the skeleton depends on the choice of the statistical model, which is subjective [42]. This distinction between deterministic and noisy dynamics may be fundamentally misleading, since the impact of noise can vary over time and be uncorrelated with system stability [42]: noise can paradoxically render the “true” deterministic skeleton irrelevant while stabilizing the dynamics, or it can lead to less predictable behavior [38]. The decision of which time series are too noisy for CCM is an important, incompletely explored problem [18].

If an ecologist were confident that observed dynamics reflected steady-state behavior, uncertainties in the methodology of attractor reconstruction still suggest caution. We tested four different methods of selecting the lag-embedding. Even with steady-state, nearly deterministic dynamics, they gave different results (Fig. S2). Decades of research on methods of attractor reconstruction show the continued difficulty of justifying a particular approach [21, 24, 25, 43, 44]. Reconstructions from unknown systems thus currently run the risk of being ad hoc and compromising causal inference. The statistics for evaluating cross-map correlations also deserve attention. We bootstrapped and attempted to validate approaches empirically with simulated data, but the methods are not rigorously grounded in a probabilistic framework such as those common to mechanistic modeling [45]. Extending the approach to explicitly link nonlinear dynamics with process and observation noise in a probabilistic framework has the potential to put the method on a sounder footing.

Of the many factors that might explain the contrasting results for childhood infections in two cities, biological explanations thus seem the least likely. Although there is evidence that measles increases susceptibility to other pathogens [26], and that measles and pertussis compete for susceptible hosts [27], the CCM analyses did not consistently support either hypothesis. It is difficult to imagine a parsimonious mechanism by which the inferred interactions might be plausible. Different rates or modes of transmission for each disease in each city might lead to varying patterns of infection in different subpopulations, which would affect interactions. We know of no support for this hypothesis. In contrast, we cannot rule out nonstationarity in the dynamics, which could arise from changes in birth rates, mobility, and behavior during this period [46]. Process noise, implying the omission of important state variables and poor resolution of the underlying deterministic attractor, could also affect performance. Errors in attractor reconstruction are another possibility. Except for pertussis, different delay-embeddings were selected for each pathogen in each city, and an alternative method of attractor reconstruction yielded even more divergent results. Finally, we cannot account for the effects of short time series and measurement error.

Detecting causality, which carries an epistemologically strong notion of truth, remains challenging in the face of real data from a complex world. We continue to question the value of coming to any strong conclusions regarding causality without additional constraining evidence beyond observational time-series data. Despite these limits, state-space reconstruction, and model-free methods in general, may still be very effective at prediction under many circumstances. Prediction, we note, is epistemologically straightforward and operationally useful even without knowledge of the true underlying structure of a system, and it does not

require deciding a priori what the best method is for the moment (model-based, model-free, or hybrid): the proof, dumb as it may be, is in the prediction.

Beyond its statistical practicalities, the prospect of applying state-space reconstruction to causal inference touches on unsettled questions in ecology. Are systems approximately deterministic and steady-state, and how could we tell? Mechanistic models remain the only option for predicting previously unobserved regime shifts in complex or rapidly evolving systems, and they are probably still useful for causal inference in these cases too. The balance hangs partly on the degree to which natural processes are fundamentally ordered and at equilibrium [47], and also on how we draw the boundaries around our systems.

Acknowledgements

We thank Mercedes Pascual, Lauren Childs, Greg Dwyer, and Nicolas Brunel for helpful comments.

Authors' contributions

Both authors planned the study and analyzed the results. EB wrote the software. SC wrote the first draft of the manuscript. Both authors contributed substantially to revisions and gave final approval for publication.

Competing interests

We declare we have no competing interests.

Funding

This work was supported in part by the University of Chicago Big Ideas Generator, and was completed in part with resources provided by the University of Chicago Research Computing Center.

4 Methods

4.1 Dynamical model

We modeled the dynamics of two pathogen strains under variable amounts of competition and process noise. The state variables in the system are the hosts' statuses with respect to each strain [48]. Hosts can be susceptible (S_i), infected (I_i), or recovered and immune (R_i) to each strain i . The deterministic model has the form:

$$\frac{dS_i}{dt} = \mu - S_i \sum_j \sigma_{ij} \beta_j(t) I_j - \mu S_i \quad (1)$$

$$\frac{dI_i}{dt} = \beta_i(t) S_i I_i - (\nu_i + \mu) I_i \quad (2)$$

$$\frac{dR_i}{dt} = \nu_i I_i + S_i \sum_{j \neq i} \sigma_{ij} \beta_j(t) I_j - \mu R_i \quad (3)$$

$$\beta_i(t) = \beta_i \left(1 + \epsilon \sin \left[\frac{2\pi}{\psi} (t - \psi) \right] \right) \quad (4)$$

$$S_i + I_i + R_i = 1 \quad (5)$$

Hosts enter the susceptible class for strain i through the birth (and death) rate μ . They leave through infection with strain i ($S_i \rightarrow I_i$), infection with strain j that elicits cross-immunity to i ($S_i \rightarrow R_i$), or death. The per capita transmission rate, $\beta_i(t)$, depends on a mean strain-specific rate, β_i , and a sinusoidal forcing function defined by a shared period, ψ . The amplitude of forcing, ϵ , is constant across strains. Infected hosts recover at rate ν_i ($I_i \rightarrow R_i$). The immune host class grows through these recoveries and also from the fraction of susceptible hosts, S_i , contacting infected hosts, I_j , who develop cross-immunity, σ_{ij} ($0 < \sigma_{ij} < 1$). Immunity of this form has been described as “polarizing” because σ_{ij} of hosts S_i contacting infecteds I_j become completely immune (non-susceptible) to strain i , while $1 - \sigma_{ij}$ remain completely susceptible. This cross-immunity is a form of competition that determines the directions of interaction between strains: when $\sigma_{ij} > 0$, strain j drives strain i .

Process noise on the per capita transmission rate produces stochastic differential equations in Ito form:

$$dS_i = [\mu - \mu S_i] dt - S_i \sum_j \sigma_{ij} \beta_j(t) I_j [dt + \eta dW_{t,j}] \quad (6)$$

$$dI_i = \beta_i(t) S_i I_i [dt + \eta dW_{t,i}] - [\nu_i + \mu] I_i dt \quad (7)$$

$$dR_i = [\nu_i I_i - \mu R_i] dt + S_i \sum_{j \neq i} \sigma_{ij} \beta_j(t) I_j [dt + \eta dW_{t,j}] \quad (8)$$

where the W_i are independent Wiener processes, one for each pathogen i , and η represents the standard deviation of the noise as a fraction of the deterministic transmission rate.

The observations consist of the number of new cases or incidence over some interval. Cumulative cases c_i at time t were obtained by summing the $S_i \rightarrow I_i$ transitions from the start of the simulation through time t . The incidence over times $t - \Delta t_{\text{obs}}$ to t , written as $C(t)$ for convenience, is given by the difference in cumulative cases:

$$C_i(t) = c_i(t_2) - c_i(t_1) \quad (9)$$

$$dc_i = \beta_i(t) S_i I_i [dt + \eta dW_{t,i}] \quad (10)$$

4.2 Simulation

The equations were solved numerically using the Euler-Maruyama method with a fixed step size. The step size was chosen to be less than the smallest within-run harmonic mean step size across deterministic,

adaptive-step size pilot runs performed across the range of parameter space being studied. When numerical errors arose during transients, the step size was reduced further until the numerical issues disappeared.

Except where noted, the model was simulated with random initial conditions, and 1000 years of monthly observations were obtained from steady state conditions. The use of random initial conditions minimizes arbitrary bias in the simulated dynamics. From visual inspection of dynamics, the transient phase lasted much less than 1000 years. Time series were obtained from years 2000-3000.

4.3 Cross-mapping

Convergent cross-mapping (CCM) is a method for inferring causality in deterministic systems via delay embedding [16]. Takens' theorem holds that, for an E -dimensional system, the attractor for the state space represented by delay vectors in a single variable X , $\mathbf{x}(t) = \{X(t), X(t - \tau_1), X(t - \tau_2), \dots, X(t - \tau_{E-1})\}$, is topologically equivalent to the E -dimensional attractor for variables X_1, \dots, X_E . In the limit of infinite data, the full E -dimensional attractor can be reconstructed perfectly from a one-dimensional time series. Therefore, because $\mathbf{x}(t)$ contains complete information about the system's dynamics, if Y is part of the same system and thus causally drives X , observations of $\mathbf{x}(t) \rightarrow Y(t - \ell)$, for a fixed lag ℓ , can be used to reconstruct unobserved values of $Y(t)$ from new observations of $\mathbf{x}(t)$ (Fig. 1).

To evaluate whether Y drives X , we construct “libraries” of observations of $\mathbf{x}(t) \rightarrow y(t - \ell)$. For a particular library, we treat each value of $Y(t)$ as unobserved, and reconstruct its value $\hat{Y}(t)$ by identifying the $E + 1$ nearest neighbors to $\mathbf{x}(t)$ in the library, $\mathbf{x}(t_i)$, for t_1, \dots, t_{E+1} , and calculating $\hat{Y} = \sum_{i=1}^{E+1} w_i Y(t_i)$. In order to avoid predictability due to system autocorrelation rather than dynamical coupling, neighbors are restricted to be separated in time by at least three times the delay at which the autocorrelation drops below $1/e$. Weights are calculated from the Euclidean distances d_i between $\mathbf{x}(t)$ and $\mathbf{x}(t_i)$, with w_i proportional to $\exp\left(-\frac{d_i}{d_0}\right)$, where d_0 is the distance to the nearest neighbor.

The cross-map correlation ρ measures how well values of Y can be reconstructed from values of X , and is defined as the Pearson correlation coefficient between reconstructed values $\hat{Y}(t)$ and actual values $Y(t)$ across the entire time series. Given library size L and lag ℓ , we generate a distribution of cross-map correlations ρ by bootstrap-sampling libraries mapping delay vectors $\mathbf{x}(t)$ to values $Y(t - \ell)$ and then computing the cross-map correlation for each sampled library. We use the bootstrap distribution of cross-map correlation as the basis for statistical criteria for causality.

4.4 Criteria for causality

We infer causality using two primary criteria involving the cross-map correlation ρ [16, 17]: (1) whether ρ increases with L for a fixed lag ℓ , and (2) whether ρ is positive and maximized at a negative temporal lag ℓ . We also consider a weaker alternative to the first criterion, which is simply whether ρ is positive.

Criterion 1 If Y drives X , then increasing the library size L should improve predictions of $\mathbf{x}(t)$ as measured by ρ [16] for fixed lag $\ell = 0$. The first criterion tests for this increase in ρ with L . We calculate ρ at $L_{\min} = E + 2$, the smallest library that will contain $E + 1$ nearest neighbors for delay vectors $\mathbf{x}(t)$, and at L_{\max} , the total number of delay vectors $\mathbf{x}(t)$ in the time series. An increase in ρ is indicated by a lack

of overlap between the distributions at $L_{\min} = E + 2$, the smallest library that will have $E + 1$ neighbors for most points, and L_{\max} , the largest possible library given the time-series length and delay embedding parameters E and τ .

Criterion 2 If Y strongly drives X , cross-map correlation at $\ell = 0$ may yield a false positive when testing for X driving Y , but because information is transferred forwards in time from Y to X , the cross-map correlation should be maximized at a negative lag ℓ [17]. The second criterion simply requires that, to infer that Y drives X , the cross-map correlation ρ be maximized at a negative cross-map lag ℓ and be positive. In other words, not only must X contain information about Y , but this information must be greatest for past states of Y , reflecting the correct temporal direction for causality.

4.5 Statistical tests for causality criteria

The theory underlying CCM assumes completely deterministic interactions and infinite data. If Y drives X in the absence of noise, the correlation ρ between the reconstructed and observed states of Y should converge to one with infinite samples of X . In practice, if X and Y share a complex (e.g., chaotic) attractor, time series of X may not be long enough to see convergence [16].

The presence of observation and/or process noise violates the deterministic assumptions and prevents ρ from ever reaching 1. Nonetheless, a detectable increase in the correlation ρ with the library length L (for Criterion 1), or a maximum and positive correlation at negative lag (for Criterion 2), may suffice to demonstrate that X drives Y in natural systems. It is important to note that we have no formal theoretical justification for such statistical heuristics.

Our statistics are based on the distributions obtained from bootstrapping. For Criterion 1, which tests for an increase in $\rho(L)$, we perform a nonparametric test of whether $\rho(L_{\max})$, obtained at the largest library length is greater than $\rho(L_{\min})$, obtained at the smallest library length. The p-value for this test is calculated as the probability that $\rho(L_{\max})$ is not greater than $\rho(L_{\min})$, and calculate the p-value directly from the sampled distributions. We also consider a weaker alternative, testing simply whether ρ is significantly positive.

For Criterion 2, which tests whether the best cross-map lag is negative and thus indicates the correct causal direction in time, we perform a similar nonparametric test. We identify the negative cross-map lag $\ell^{(-)}$ with the highest median correlation, $\rho(\ell^{(-)})$ as well as the nonnegative cross-map lag $\ell^{(0+)}$ with the highest median correlation. The p-value for this test is calculated as the probability that $\rho(\ell^{(-)})$ is not greater than $\rho(\ell^{(0+)})$.

4.6 Choice of delay and embedding dimension

The theory underlying attractor reconstruction works with any E -dimensional projection of a one-dimensional time series, which can be generated in many ways from lags of the time series. In simulated, deterministic models, E can be known perfectly, but the best projection may be system-dependent. In systems with process noise, unknown dynamics, and/or finite observations, there is no clearly superior method to select the appropriate projection [24, 25, 43, 49–51].

We accommodated this uncertainty by using four different methods. Two methods infer the best delay-embedding for each interaction by maximizing the ability of one variable, the driven variable, to predict itself (akin to nonlinear forecasting [44, 52]). The third method instead uses the delay-embedding that maximizes the cross-mapping correlation ρ for each interaction. Three of the four methods use uniform embeddings, identifying E and a fixed delay τ , and the other uses a nonuniform embedding, identifying a series of specific delays τ_1, τ_2 , etc., whose length determines E .

1. *Univariate prediction method*: By default, for each causal interaction ($C_i \rightarrow C_j$), E and τ are chosen to maximize the one-step-ahead univariate prediction ρ at L_{\max} for the driven variable (C_j) based on its own time series.
2. *Maximum cross-correlation method*: As an alternative, E and τ are chosen to maximize the mean cross-map correlation ρ at L_{\max} for each causal interaction being tested, for each time series.
3. *Random projection method*: A recently proposed method based on random projection of delay coordinates sidesteps the problem of choosing optimal delays [21]. Instead, for a given E , all delays up to a maximum delay τ_{\max} are projected onto an E -dimensional vector via multiplication by a random projection matrix. E is chosen to maximize the cross-map correlation ρ .
4. *Nonuniform method*: For each driven variable C_j , starting with $\tau_0 = 0$, additional delays τ_1, τ_2, \dots are chosen iteratively to maximize the directional derivative to nearest neighbors when the new delay is added [24]. The delays are bounded by the optimal uniform embedding based on a cost function that penalizes irrelevant information [25]. This method can be seen as a nonuniform extension of the method of false nearest neighbors [53].

4.7 Code

Code implementing the state-space reconstruction methods is publicly available at <https://github.com/cobeylab/pyembedding>. The complete code for the analysis and figures is publicly available at https://github.com/cobeylab/causality_manuscript; individual analyses include references to the Git commit version identifier in the ‘pyembedding’ repository. The simulated time series on which the analyses were performed are available from the authors on request.

4.8 Data on childhood infections

Time series were obtained from L2-level data maintained by Project Tycho [28]. All available cases of measles, mumps, pertussis, polio, scarlet fever, and varicella were obtained from the first week of 1906 through the last week of 1953 for New York City and Chicago. Pertussis data were truncated in the 26th week of 1948. Incidence was calculated by dividing weekly cases by a spline fit to each city’s population size, as reported by the U.S. Census.

References

- [1] Matt J. Keeling and Pejman Rohani. *Modeling Infectious Diseases in Humans and Animals*. Princeton University Press, 2011.

- [2] Roy M. & Robert M. May Anderson. *Infectious Diseases of Humans. Dynamics and Control*. Oxford University Press, 1995.
- [3] W. O. Kermack and A. G. McKendrick. A contribution to the mathematical theory of epidemics. *Proceedings of the Royal Society A: Mathematical, Physical and Engineering Sciences*, 115(772):700–721, aug 1927.
- [4] R. Ross. *The Prevention of malaria*. J. Murray, 1910.
- [5] Karina Laneri, Anindya Bhadra, Edward L. Ionides, Menno Bouma, Ramesh C. Dhiman, Rajpal S. Yadav, and Mercedes Pascual. Forcing versus feedback: Epidemic malaria and monsoon rains in northwest india. *PLoS Comput Biol*, 6(9):e1000898, sep 2010.
- [6] B. F. Finkenstädt and B. T. Grenfell. Time series modelling of childhood diseases: a dynamical systems approach. *J. R. Stat. Soc. Ser. C*, 49(2):187–205, 2000.
- [7] P E Fine and J A Clarkson. Measles in England and Wales–I: An analysis of factors underlying seasonal patterns. *Int J Epidemiol*, 11(1):5–14, Mar 1982.
- [8] Kenneth P. Burnham and David R. Anderson. *Model Selection and Multimodel Inference: A Practical Information-Theoretic Approach*. Springer, 2003.
- [9] D. He, E. L. Ionides, and A. A. King. Plug-and-play inference for disease dynamics: measles in large and small populations as a case study. *Journal of The Royal Society Interface*, 7(43):271–283, jun 2009.
- [10] Peter Yodzis. The indeterminacy of ecological interactions as perceived through perturbation experiments. *Ecology*, 69(2):508–515, 1988.
- [11] Matthew B. Thomas Simon N. Wood. Super-sensitivity to structure in biological models. *Proceedings: Biological Sciences*, 266(1419):565–570, 1999.
- [12] C. W. J. Granger. Investigating causal relations by econometric models and cross-spectral methods. *Econometrica*, 37(3):424, aug 1969.
- [13] Johannes Schumacher, Thomas Wunderle, Pascal Fries, Frank Jäkel, and Gordon Pipa. A statistical framework to infer delay and direction of information flow from measurements of complex systems. *Neural Computation*, 27(8):1555–1608, aug 2015.
- [14] Joris M. Mooij, Jonas Peters, Dominik Janzing, Jakob Zscheischler, and Bernhard Schölkopf. Distinguishing cause from effect using observational data: methods and benchmarks. *CoRR*, abs/1412.3773, 2014.
- [15] Oliver Stegle, Dominik Janzing, Kun Zhang, Joris M. Mooij, and Bernhard Schölkopf. Probabilistic latent variable models for distinguishing between cause and effect. In J.D. Lafferty, C.K.I. Williams, J. Shawe-Taylor, R.S. Zemel, and A. Culotta, editors, *Advances in Neural Information Processing Systems 23*, pages 1687–1695. Curran Associates, Inc., 2010.
- [16] G. Sugihara, R. May, H. Ye, C. h. Hsieh, E. Deyle, M. Fogarty, and S. Munch. Detecting causality in complex ecosystems. *Science*, 338(6106):496–500, sep 2012.
- [17] Hao Ye, Ethan R. Deyle, Luis J. Gilarranz, and George Sugihara. Distinguishing time-delayed causal interactions using convergent cross mapping. *Sci. Rep.*, 5:14750, oct 2015.

- [18] Adam Thomas Clark, Hao Ye, Forest Isbell, Ethan R. Deyle, Jane Cowles, G. David Tilman, and George Sugihara. Spatial convergent cross mapping to detect causal relationships from short time series. *Ecology*, 96(5):1174–1181, 2015.
- [19] Floris Takens. Detecting strange attractors in turbulence. In David Rand and Lai-Sang Young, editors, *Dynamical Systems and Turbulence, Warwick 1980*, volume 898 of *Lecture Notes in Mathematics*, pages 366–381. Springer Berlin Heidelberg, 1981.
- [20] L. Kocarev and U. Parlitz. Generalized synchronization, predictability, and equivalence of unidirectionally coupled dynamical systems. *Phys. Rev. Lett.*, 76(11):1816–1819, mar 1996.
- [21] Satoshiro Tajima, Toru Yanagawa, Naotaka Fujii, and Taro Toyoizumi. Untangling brain-wide dynamics in consciousness by cross-embedding. *PLOS Computational Biology*, 11(11):e1004537, nov 2015.
- [22] Anastasios A. Tsonis, Ethan R. Deyle, Robert M. May, George Sugihara, Kyle Swanson, Joshua D. Verbeten, and Geli Wang. Dynamical evidence for causality between galactic cosmic rays and interannual variation in global temperature. *Proceedings of the National Academy of Sciences*, 112(11):3253–3256, mar 2015.
- [23] Sarah Cobey. Pathogen evolution and the immunological niche. *Annals of the New York Academy of Sciences*, 1320(1):1–15, 2014.
- [24] Chetan Nichkawde. Optimal state-space reconstruction using derivatives on projected manifold. *Phys. Rev. E*, 87:022905, Feb 2013.
- [25] L. C. Uzal, G. L. Grinblat, and P. F. Verdes. Optimal reconstruction of dynamical systems: A noise amplification approach. *Physical Review E*, 84(1), jul 2011.
- [26] M. J. Mina, C. J. E. Metcalf, R. L. de Swart, A. D. M. E. Osterhaus, and B. T. Grenfell. Long-term measles-induced immunomodulation increases overall childhood infectious disease mortality. *Science*, 348(6235):694–699, may 2015.
- [27] P. Rohani, C. J. Green, N. B. Mantilla-Beniers, and B. T. Grenfell. Ecological interference between fatal diseases. *Nature*, 422(6934):885–888, apr 2003.
- [28] Willem G. van Panhuis, John Grefenstette, Su Yon Jung, Nian Shong Chok, Anne Cross, Heather Eng, Bruce Y. Lee, Vladimir Zadorozhny, Shawn Brown, Derek Cummings, and Donald S. Burke. Contagious diseases in the united states from 1888 to the present. *New England Journal of Medicine*, 369(22):2152–2158, nov 2013.
- [29] Jeffrey Shaman, Virginia E. Pitzer, Cécile Viboud, Bryan T. Grenfell, and Marc Lipsitch. Absolute humidity and the seasonal onset of influenza in the continental united states. *PLoS Biology*, 8(2):e1000316, feb 2010.
- [30] Sonia Altizer, Andrew Dobson, Parvize Hosseini, Peter Hudson, Mercedes Pascual, and Pejman Rohani. Seasonality and the dynamics of infectious diseases. *Ecology Letters*, 9(4):467–484, mar 2006.
- [31] C. J. E. Metcalf, O. N. Bjornstad, B. T. Grenfell, and V. Andreasen. Seasonality and comparative dynamics of six childhood infections in pre-vaccination copenhagen. *Proceedings of the Royal Society B: Biological Sciences*, 276(1676):4111–4118, sep 2009.

- [32] David Alonso, Alan J. McKane, and Mercedes Pascual. Stochastic amplification in epidemics. *Journal of The Royal Society Interface*, 4(14):575–582, dec 2006.
- [33] H. T.H Nguyen and P. Rohani. Noise, nonlinearity and seasonality: the epidemics of whooping cough revisited. *Journal of The Royal Society Interface*, 5(21):403–413, apr 2008.
- [34] H. B. Wilson D. A. Rand. Chaotic stochasticity: A ubiquitous source of unpredictability in epidemics. *Proceedings: Biological Sciences*, 246(1316):179–184, 1991.
- [35] Pejman Rohani, Matthew J. Keeling, and Bryan T. Grenfell. The interplay between determinism and stochasticity in childhood diseases. *The American Naturalist*, 159(5):469–481, 2002.
- [36] Richard P. Boland, Tobias Galla, and Alan J. McKane. Limit cycles, complex floquet multipliers, and intrinsic noise. *Physical Review E*, 79(5), may 2009.
- [37] A. J. McKane and T. J. Newman. Predator-prey cycles from resonant amplification of demographic stochasticity. *Phys. Rev. Lett.*, 94(21), jun 2005.
- [38] Peter Turchin. *Complex Population Dynamics: A Theoretical/Empirical Synthesis (MPB-35) (Monographs in Population Biology)*. Princeton University Press, 2003.
- [39] R. M. Nisbet W. S. C. Gurney. Single-species population fluctuations in patchy environments. *The American Naturalist*, 112(988):1075–1090, 1978.
- [40] R. Durrett and S. Levin. The importance of being discrete (and spatial). *Theoretical Population Biology*, 46(3):363–394, dec 1994.
- [41] Anthony R. Ives and Vasilis Dakos. Detecting dynamical changes in nonlinear time series using locally linear state-space models. *Ecosphere*, 3(6):art58, jun 2012.
- [42] Peter Turchin Stephen Ellner. Chaos in a noisy world: New methods and evidence from time-series analysis. *The American Naturalist*, 145(3):343–375, 1995.
- [43] Martin Casdagli, Stephen Eubank, J.Doyne Farmer, and John Gibson. State space reconstruction in the presence of noise. *Physica D: Nonlinear Phenomena*, 51(1-3):52–98, aug 1991.
- [44] George Sugihara and Robert M. May. Nonlinear forecasting as a way of distinguishing chaos from measurement error in time series. *Nature*, 344(6268):734–741, apr 1990.
- [45] Ray Hilborn and Marc Mangel. *The Ecological Detective: Confronting Models with Data*. Princeton University Press, 1997.
- [46] D. J. Earn. A simple model for complex dynamical transitions in epidemics. *Science*, 287(5453):667–670, jan 2000.
- [47] Alan Hastings. Transients: the key to long-term ecological understanding? *Trends in Ecology & Evolution*, 19(1):39–45, jan 2004.
- [48] J.R. Gog and J. Swinton. A status-based approach to multiple strain dynamics. *J Math Biol*, 44(2):169–184, feb 2002.
- [49] Louis M. Pecora, Linda Moniz, Jonathan Nichols, and Thomas L. Carroll. A unified approach to attractor reconstruction. *Chaos*, 17(1), 2007.

Table 1: Default parameter values.

Symbol	Description	Default value
β_1, β_2	transmission rates	0.3, 0.25 d ⁻¹
σ_{12}	immunity to strain 1 from infection with 2	see text
σ_{21}	immunity to strain 2 from infection with 1	0
σ_{ii}	homologous immunity for strain i	1
μ	birth and death rate	1/30 y ⁻¹
ν	recovery rate	0.2 d ⁻¹
ϵ	amplitude of seasonal forcing	0.1
ψ	period of seasonal forcing	360 d
η	standard deviation of process noise	see text
$S(0)$	initial fraction susceptible	see text
$I(0)$	initial fraction infected	see text
Δt_{obs}	incidence and sampling interval	30 days

- [50] Liangyue Cao. Practical method for determining the minimum embedding dimension of a scalar time series. *Phys. D*, 110(1-2):43–50, December 1997.
- [51] Michael Small and C.K. Tse. Optimal embedding parameters: a modelling paradigm. *Physica D: Nonlinear Phenomena*, 194(3-4):283–296, jul 2004.
- [52] G. Sugihara. Nonlinear forecasting for the classification of natural time series. *Philosophical Transactions of the Royal Society A: Mathematical, Physical and Engineering Sciences*, 348(1688):477–495, sep 1994.
- [53] Matthew B. Kennel, Reggie Brown, and Henry D. I. Abarbanel. Determining embedding dimension for phase-space reconstruction using a geometrical construction. *Phys. Rev. A*, 45(6):3403–3411, mar 1992.

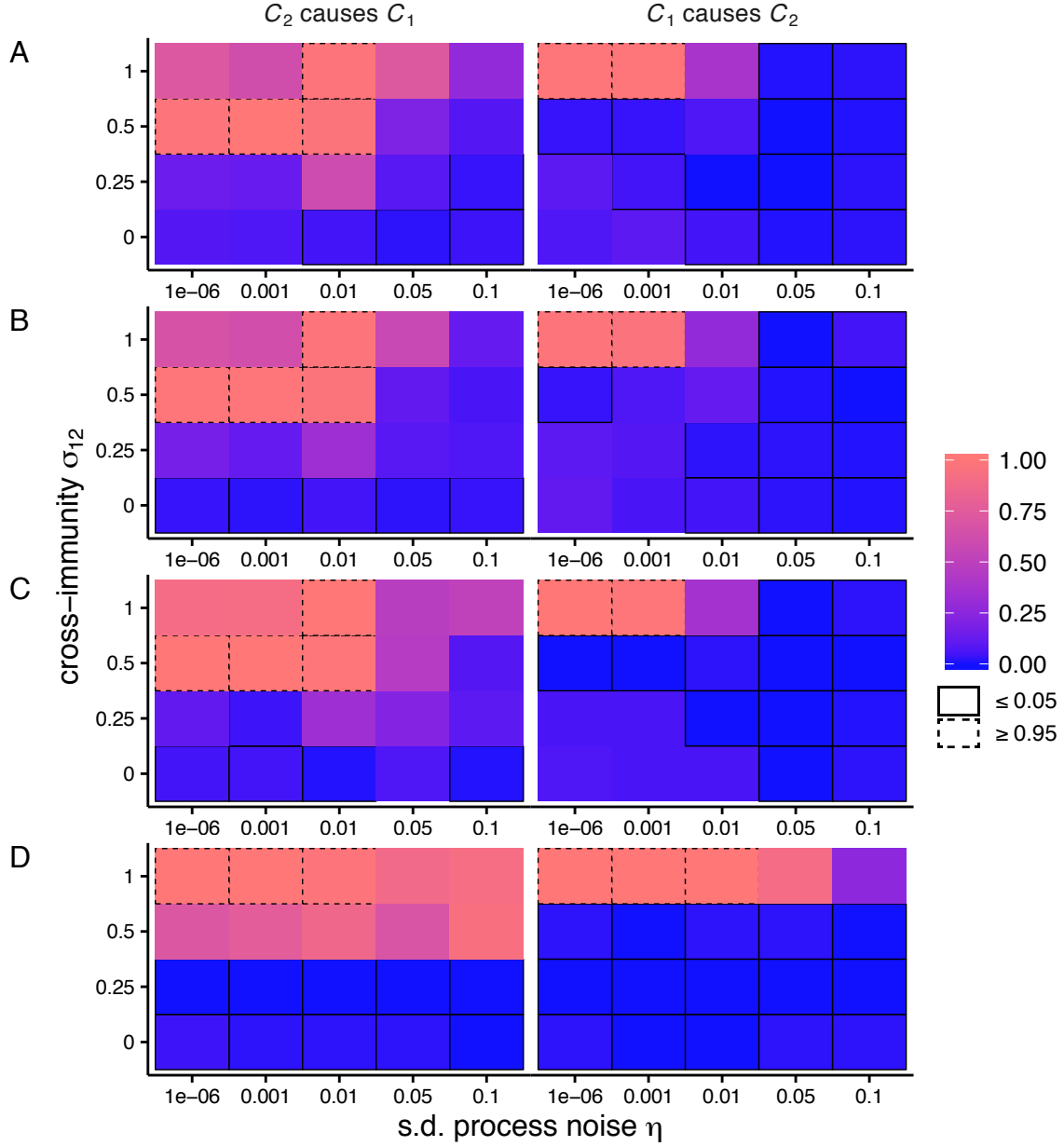


Figure S1: **Interactions detected as a function of process noise and the strength of interaction ($C_2 \rightarrow C_1$) for different types of data.** Heat maps show the fraction of 100 replicates significant for each inferred interaction for different parameter combinations. A significant increase in cross-map correlation ρ with library length L indicated a causal interaction. (A) Annual incidence, (B) prevalence strobed annually, (C) first-differenced annual incidence, and (D) monthly incidence without seasonal forcing.

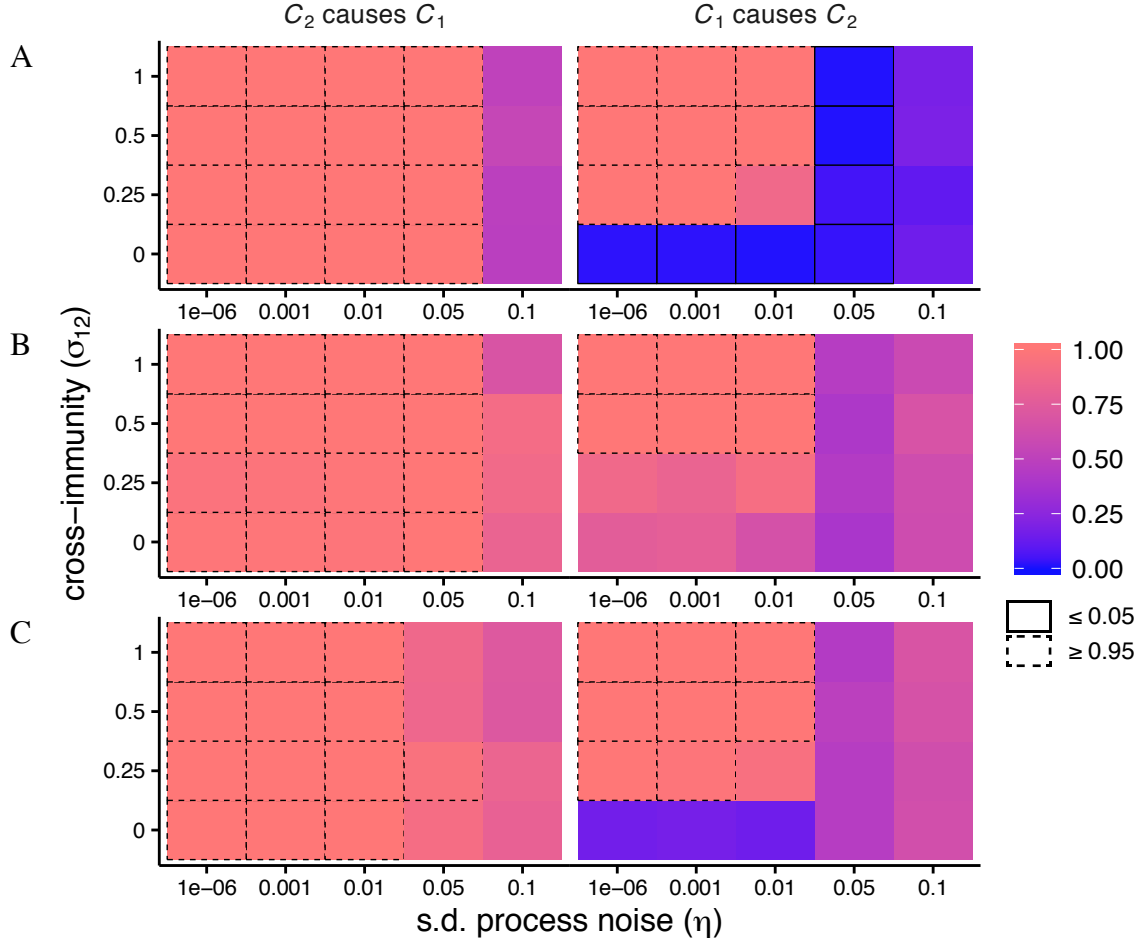


Figure S2: **Interactions detected as a function of process noise and the strength of interaction ($C_2 \rightarrow C_1$) for different delay-embedding methods.** Heat maps show the fraction of 100 replicates significant for each inferred interaction for different parameter combinations. A significant increase in cross-map correlation ρ with library length L indicated a causal interaction. Delay-embeddings were chosen by (A) nonuniform embedding, (B) random projection, or (C) maximizing the cross-map correlation ρ .

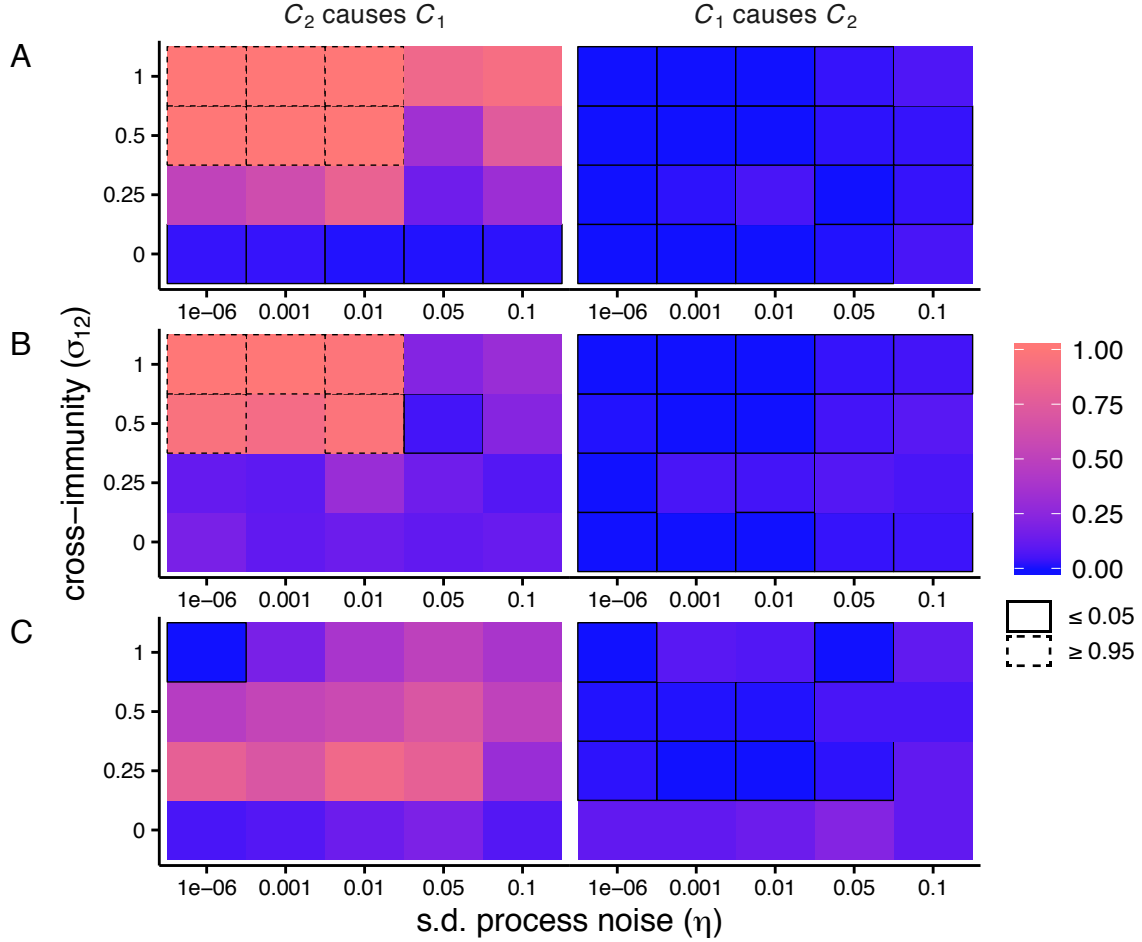


Figure S3: **Interactions detected for different types of data.** Heat maps show the fraction of 100 replicates significant for each inferred interaction for different parameter combinations. A maximum cross-map correlation ρ at a negative lag was required for inferring causal interaction. (A) Annual incidence, requiring that the maximum ρ be positive. (B) Monthly incidence, requiring that the maximum ρ be increasing. (C) Monthly incidence with identical strains ($\beta_1 = \beta_2 = 0.3$), requiring that maximum ρ be positive.

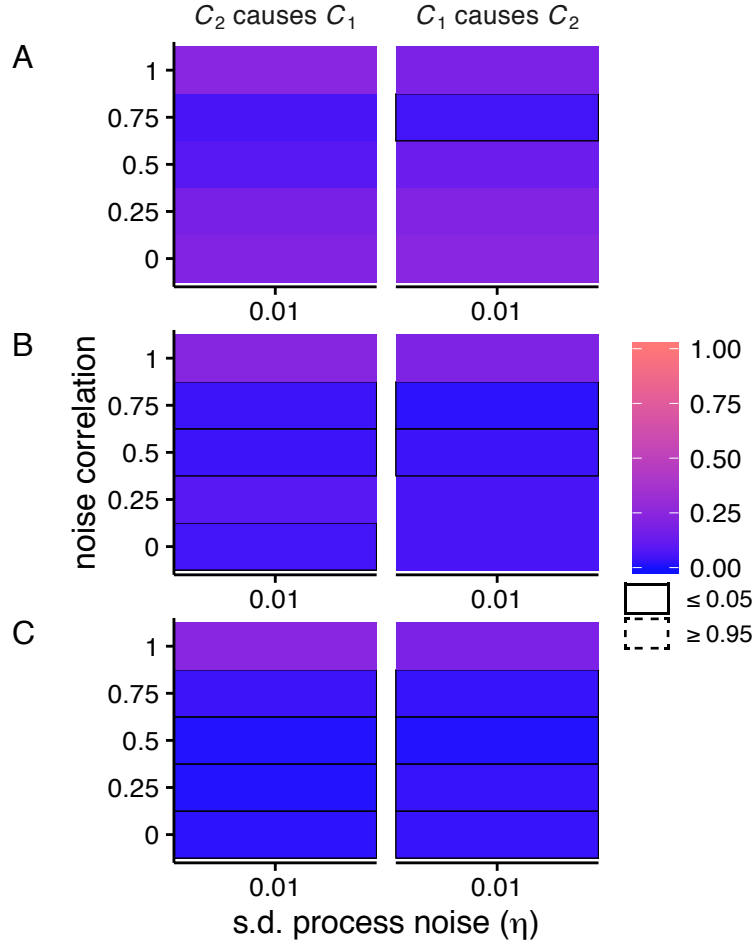


Figure S4: **Interactions detected between identical strains with correlated process noise.** Heat maps show the fraction of 100 replicates significant for each inferred interaction. A maximum cross-map correlation ρ at a negative lag was required for inferring causal interaction. Monthly (A) and annual (B) incidence, requiring that the maximum ρ be positive. (C) Monthly incidence, requiring that maximum ρ be increasing.

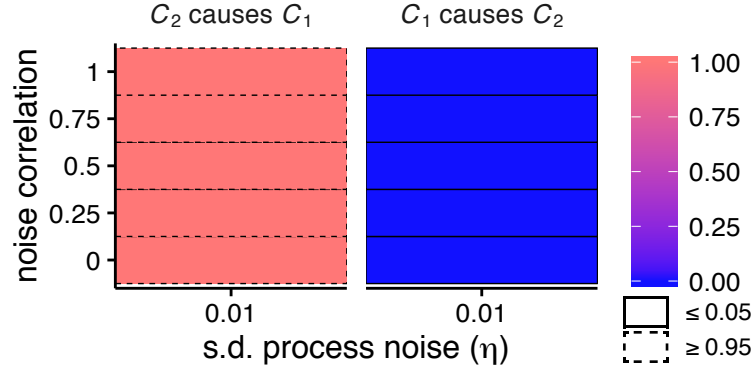


Figure S5: **Interactions detected between distinct strains with correlated process noise.** Heat maps show the fraction of 100 replicates significant for each inferred interaction. A maximum cross-map correlation ρ at a negative lag and $\rho > 0$ were required for inferring causal interaction. Results shown for monthly incidence.

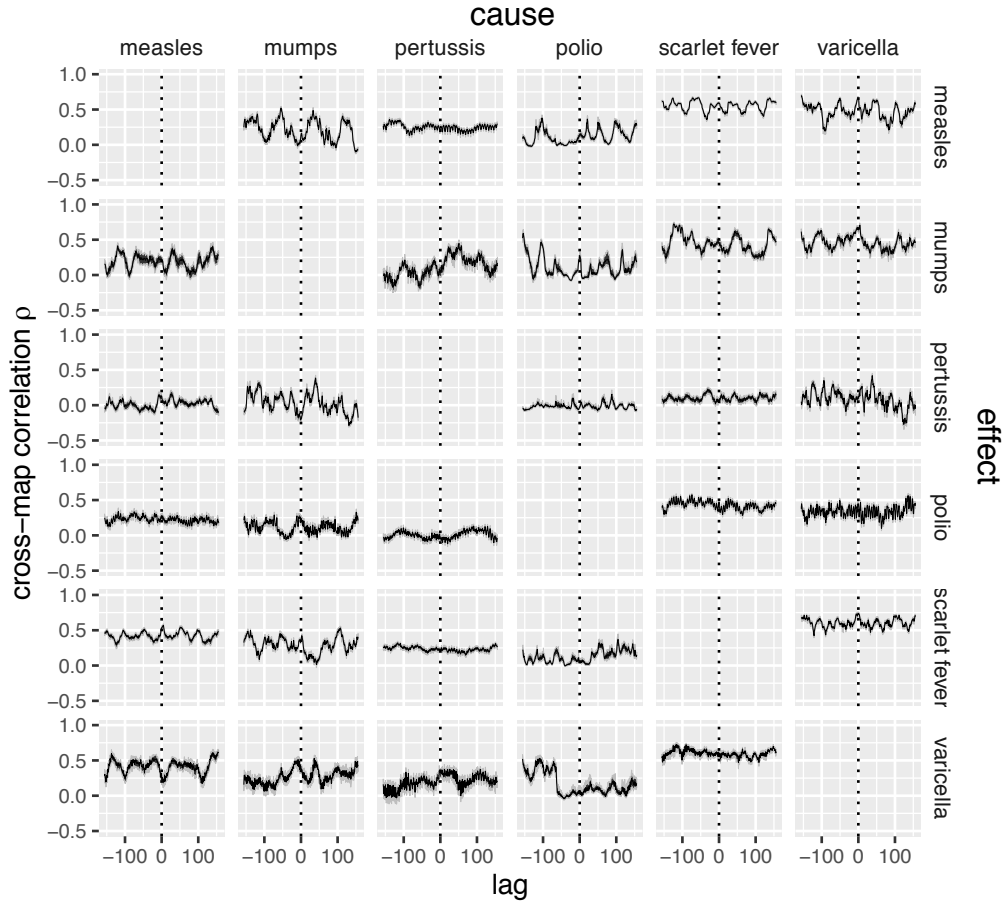


Figure S6: **Cross-map lags for New York with default (univariate) embedding.**

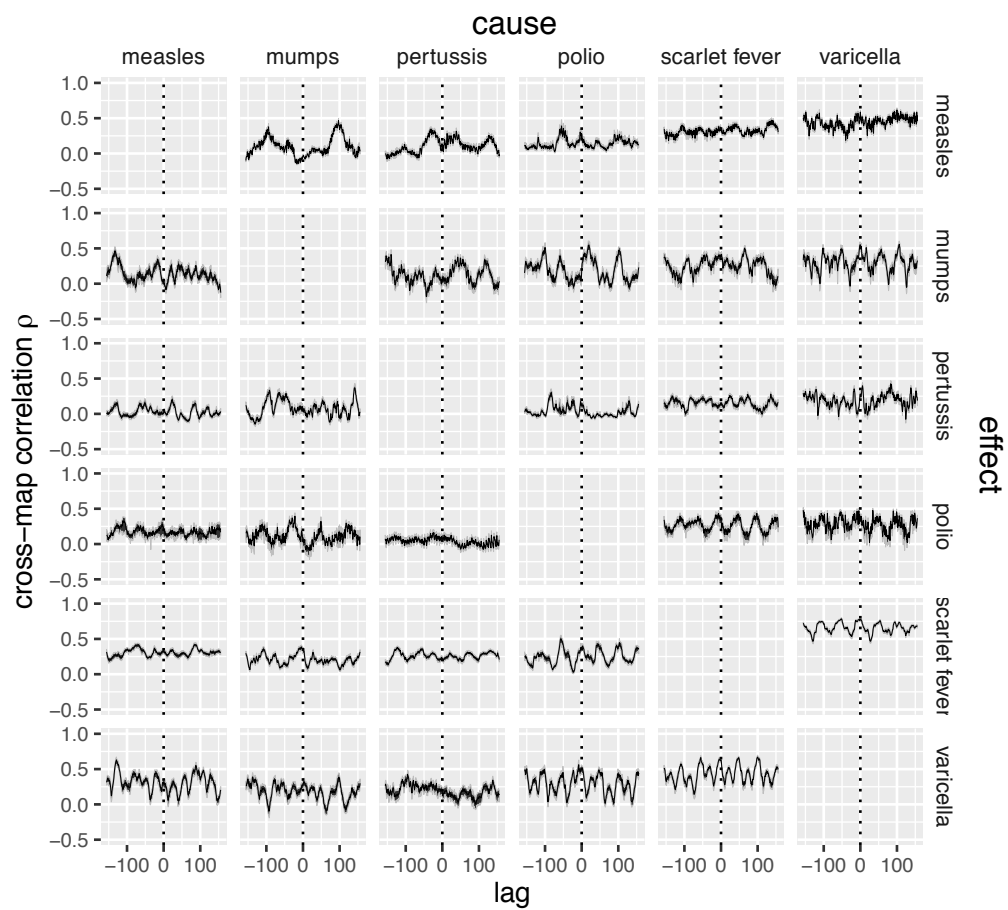


Figure S7: Cross-map lags for Chicago with default (univariate) embedding.

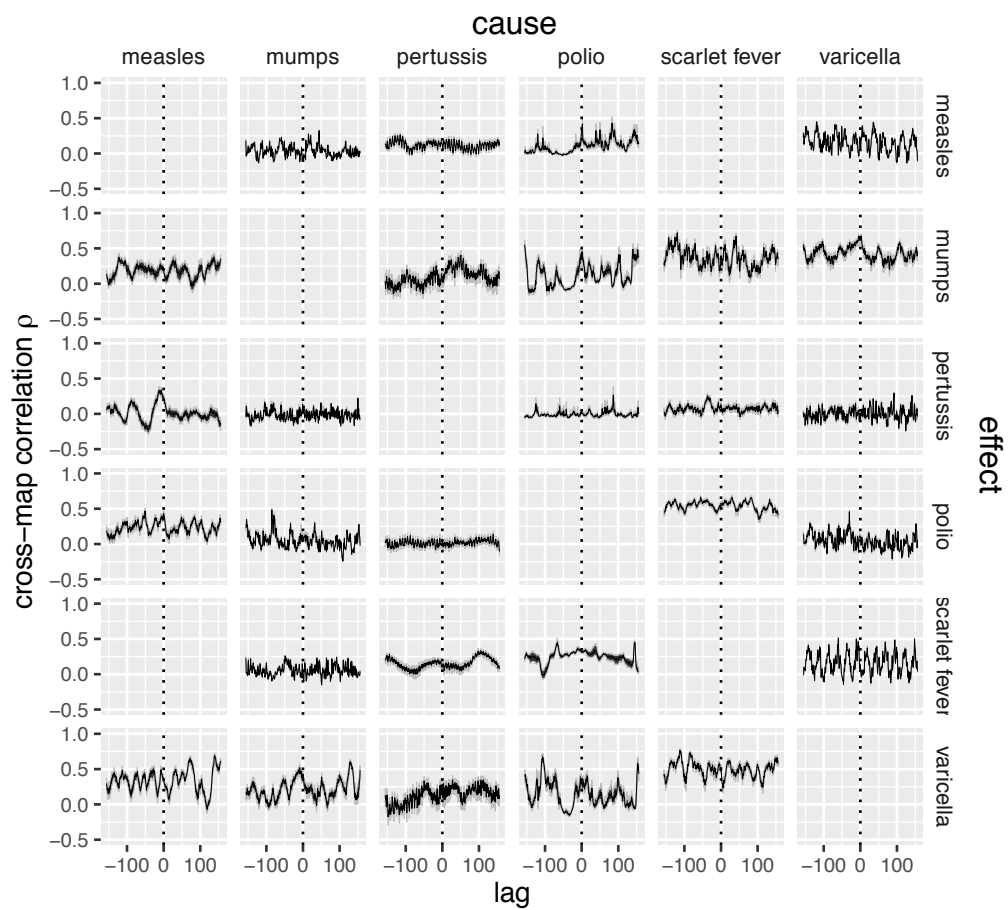


Figure S8: Cross-map lags for New York with embedding based on random projection.

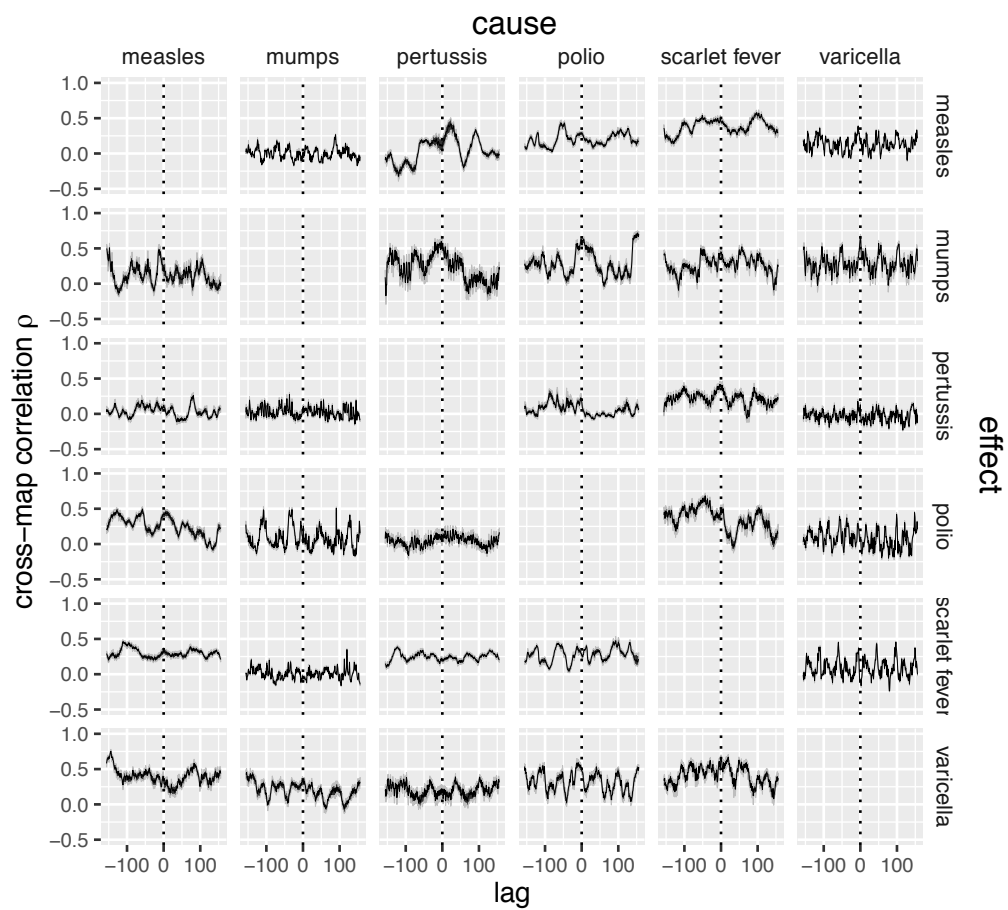


Figure S9: Cross-map lags for Chicago with embedding based on random projection.